

Debonding strands as an anchorage zone crack control method for pretensioned concrete bulb-tee girders

Emre Kizilarlan, Pinar Okumus, and Michael G. Oliva

- Using field test monitoring and finite element analysis, this paper studies whether debonding strands can successfully control cracks at the ends of pretensioned girders.
- The field monitoring was conducted during prestress release on 72 in. (1829 mm) deep concrete bulb-tee bridge girders with 0% and 25% debonding ratios and 54 in. (1372 mm) deep concrete bulb-tee bridge girders with 0%, 38%, and 62% debonding ratios and varying debonding lengths.
- Variations in girder depth, total number of strands, and debonding ratio were reviewed with the finite element analysis models.

To meet bridge load demands efficiently, pretensioned concrete bulb-tee girders are heavily prestressed in most cases. Although the pretension force is transferred gradually to concrete near girder ends, tensile stresses developing in the anchorage zones can be large enough to create cracks in relatively thin girder webs. Deeper girders with larger prestressing forces tend to have more, longer, or wider cracks.¹ When end zones are not encased in concrete diaphragms, cracks may create concerns for corrosion. Tadros et al.² recommended repairing cracks between 0.012 and 0.050 in. (0.30 and 1.27 mm) in width and rejecting girders with cracks larger than 0.050 in. in width.

Horizontal end cracks were noticed in pretensioned members in the 1960s and investigated with an experimental study by Marshall and Mattock.^{3,4} Since then, many researchers have performed analytical studies (such as the Gergely-Sozen model, strut-and-tie models, and nonlinear finite element analysis) and experimental studies to understand end-zone stresses or design reinforcement at girder ends.⁵⁻¹⁷

End, or anchorage, zone cracks can be categorized into three groups according to location and orientation: inclined web cracks (measured by the authors to be 0.004 to 0.010 in. [0.102 to 0.254 mm] wide), horizontal web cracks (measured by the authors to be 0.004 to 0.010 in. wide), and bottom-flange Y-shaped cracks (measured by the authors to be 0.02 to 0.06 in. [0.508 to 1.524 mm] wide) (**Fig. 1**).¹⁸ Out of the three groups, Y cracks are particularly concerning because they are the widest, are closest to the strands in the bulb, and can lead to corrosion.

PCI Journal (ISSN 0887-9672) V. 65, No. 5, September–October 2020.

PCI Journal is published bimonthly by the Precast/Prestressed Concrete Institute, 8770 W. Bryn Mawr Ave., Suite 1150, Chicago, IL 60631.

Copyright © 2020, Precast/Prestressed Concrete Institute. The Precast/Prestressed Concrete Institute is not responsible for statements made by authors of papers in *PCI Journal*. Original manuscripts and discussion on published papers are accepted on review in accordance with the Precast/Prestressed Concrete Institute's peer-review process. No payment is offered.

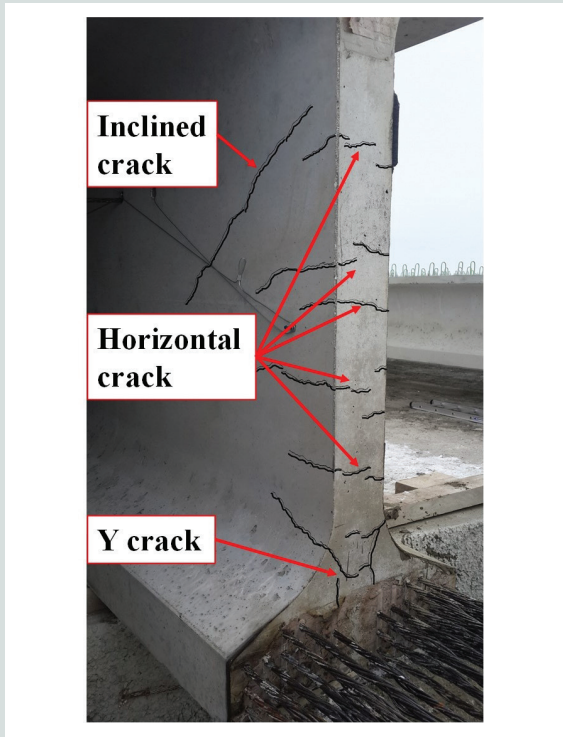


Figure 1. Inclined, horizontal, and Y cracks shown on a 72W Wisconsin bulb-tee girder. Note: Cracks are highlighted for visibility. 72W = 72 in. deep Wisconsin wide flanged bulb-tee bridge girder. 1 in. = 25.4 mm.

The most common crack control method is designing reinforcement for girder end-zone stresses.^{7-9,13,15,19} The American Association of State Highway and Transportation Officials' *AASHTO LRFD Bridge Design Specifications*²⁰ section 5.10.10 requires reinforcement to control splitting and bursting stresses. Other methods for crack control include changing strand-cutting order, vertical post-tensioning, adjusting the lifting-hoop position, and using a draped strand position.^{7-9,14,21,22} Debonding some strands over girder ends has been shown to be effective in reducing transferred prestress and controlling end-zone cracks.^{8,10,14} The majority of the studies on debonding focus on web cracks.

The main objective of this research was to determine whether debonding strands can successfully control cracks, particularly bottom-flange Y cracks, at the ends of pretensioned girders right after detensioning. Field tests were conducted on girders, with debonding ratios ranging from 0% to 62% and varying debonding lengths. This study focused on controlling Y cracks through debonding strands because Y cracks are considered the most detrimental to girder serviceability. The vertical leg of the Y crack that forms at the girder end may be caused by the eccentricity of the resultant strand forces in the bottom flange over the width of the girder (e_h in **Fig. 2**). A resultant strand force from the prestress transfer exists on each side of the bottom flange with no force at the center (because of the absence of the draped strands). These forces create a bending effect in the bottom flange. The outer edges of the flange are compressed, while the midsection is relatively uncompressed but restrained by the web where no stress transfer occurs.

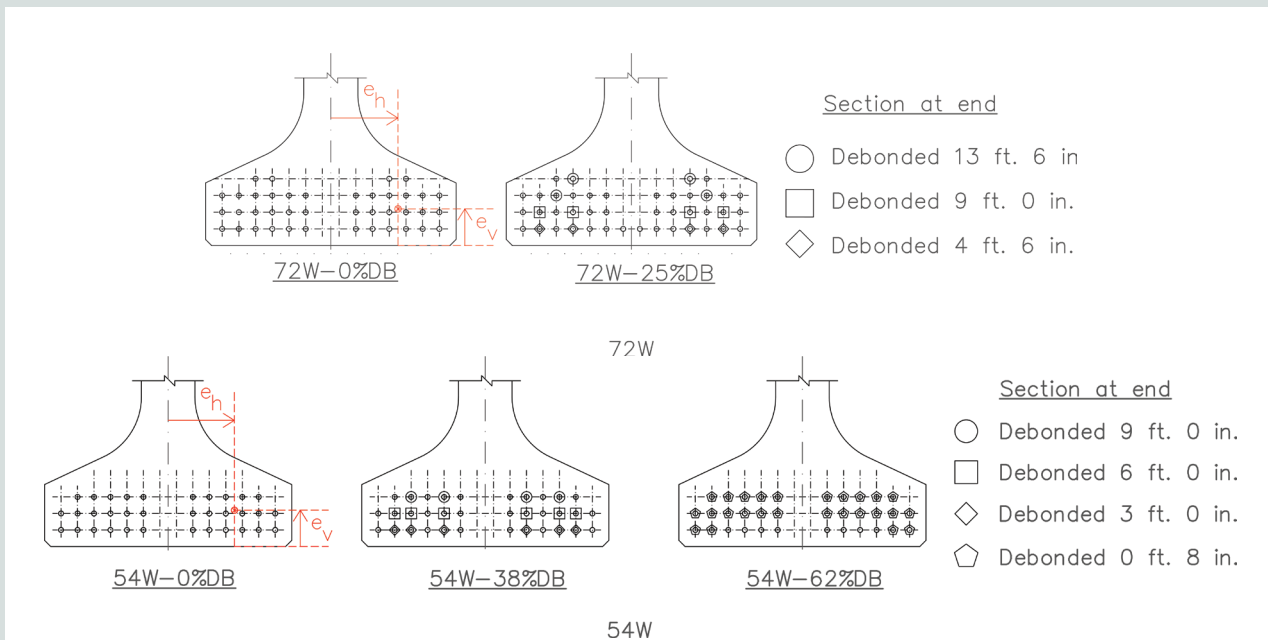


Figure 2. Strand details at 72W and 54W girder ends. Note: 54W = 54 in. deep Wisconsin wide flanged bulb-tee bridge girder; 72W = 72 in. deep Wisconsin wide flanged bulb-tee bridge girder; DB = debonding ratio; e_h = horizontal eccentricity of the bonded straight strands; e_v = vertical eccentricity of the bonded straight strands from bottom of the girders. 1 in. = 25.4 mm; 1 ft = 0.305 m.

Once a vertical crack forms at the girder end, it tends to meet the lower web crack, forming a Y crack.

Therefore, debonding should also attempt to reduce the horizontal eccentricity of force across the width of the bottom flange. Cracks, reinforcement strains, and concrete strains were measured during detensioning of 72 and 54 in. (1829 and 1372 mm) deep bulb-tee girders. The measurements were compared for girders with and without debonded strands.

The field test results were then used to validate nonlinear finite element analysis models. A parametric study was run with finite element analysis models; girder depth, total number of strands, and debonding ratio were variables.

Girders monitored

Two 72 in. (1829 mm) deep and three 54 in. (1372 mm) deep Wisconsin wide flanged bulb-tee bridge girders (72W and 54W, respectively), complying with the AASHTO LRFDF

specifications²⁰ except for the maximum allowed debonding ratio, were instrumented and monitored during prestress release. The 72W and 54W girders were built at separate precasting plants. Figure 2 shows the strand patterns and debonding of the girders. These were chosen to maximize the likelihood of end cracking. All strands were low-relaxation strands with 0.6 in. (15.24 mm) diameter and 270 ksi (1862 MPa) ultimate strength.

The girders had debonding ratios varying from 0% to 62%. Girders with no debonding were used as baselines. The girders are denoted with numbers indicating their depth (72 or 54 in. [1829 or 1372 mm]), followed by their debonding ratios (0%DB to 62%DB). **Table 1** shows the properties and reinforcement details of the girders monitored. The Wisconsin Department of Transportation (WisDOT) *Bridge Manual*²³ gives standard anchorage zone reinforcement details. In Table 1, the horizontal eccentricity and vertical eccentricity of the bonded strands refer to the eccentricity of the resultant prestress force from strands on one side of the bottom flange

Table 1. Properties and details of the instrumented girders

	72W-0%DB	72W-25%DB	54W-0%DB	54W-38%DB	54W-62%DB
Girder depth h , in.	72	72	54	54	54
Girder length, ft	154.75	154.75	125.05	125.05	125.05
Number of bonded and unbonded straight strands	40	42	34	34	34
Number of draped strands	8	6	8	8	8
Number of bonded straight strands	40	30	34	18	8
Debonding ratio, %	0	25	0	38	62
Length of debonding, ft	n/a	Staggered 4.5, 9.0, and 13.5	n/a	Staggered 3.0, 6.0, and 9.0	0.67
Horizontal eccentricity of the bonded straight strands e_h , in.	8.00	7.27	7.71	7.44	6.00
Vertical eccentricity of the bonded straight strands e_v , in.	4.40	4.27	3.88	4.00	2.00
Splitting reinforcement within $h/4$	10 no. 6 and 2 no. 4	10 no. 6 and 2 no. 4	10 no. 6	10 no. 6	10 no. 6
Ratio of splitting resistance P_r in $h/4$ to total prestressing force, %	4.56	4.56	4.79	4.79	4.79
Concrete strength at detensioning, ksi	7.81	7.02	7.82	8.14	7.98

Note: 54W = 54 in. deep Wisconsin wide flanged bulb-tee bridge girder; 72W = 72 in. deep Wisconsin wide flanged bulb-tee bridge girder; DB = debonding ratio; h = the height of girders; n/a = not applicable. No. 4 = 13M; no. 6 = 19M; 1 in. = 25.4 mm; 1 ft = 0.305 m; 1 ksi = 6.895 MPa.

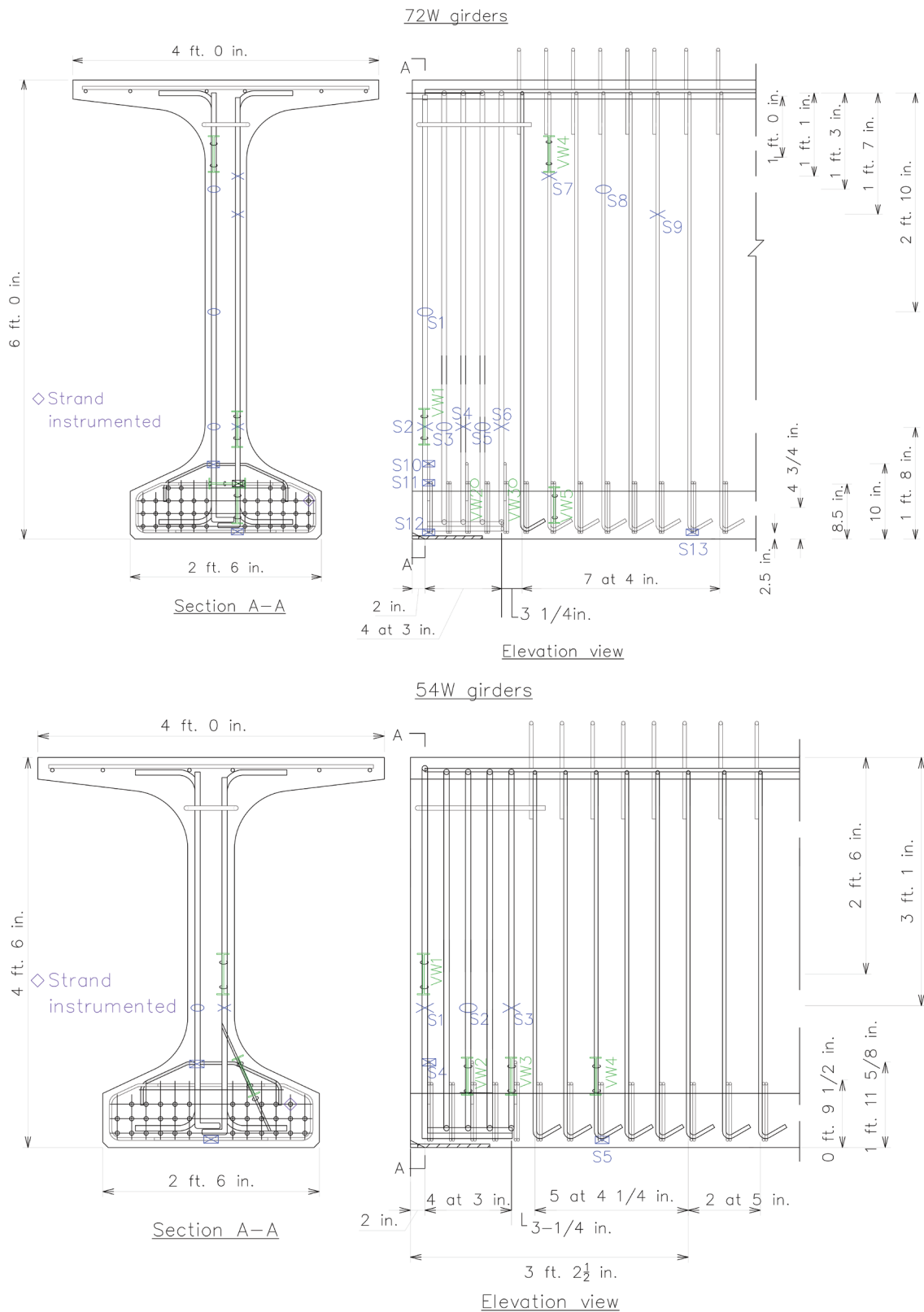


Figure 3. Location of gauges in 72W and 54W girders. Note: 54W = 54 in. deep Wisconsin wide flanged bulb-tee bridge girder; 72W = 72 in. deep Wisconsin wide flanged bulb-tee bridge girder; S = electric resistance surface gauge; VW = vibrating-wire strain gauge. 1 in. = 25.4 mm; 1 ft = 0.305 m.

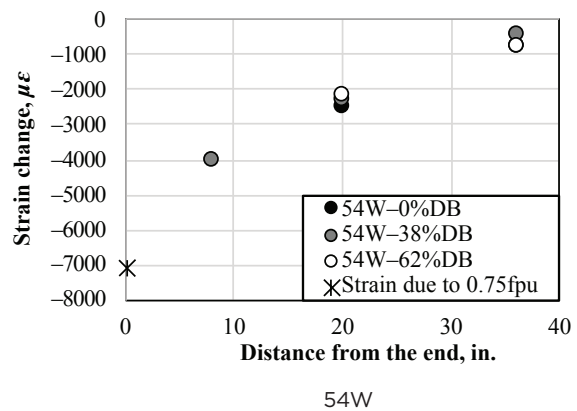
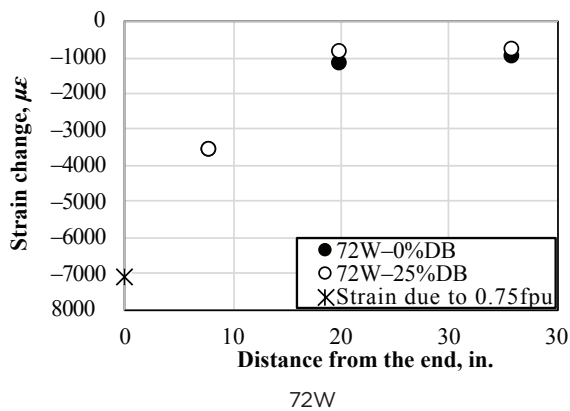


Figure 4. Strain change for 72W and 54W girders. Note: 54W = 54 in. deep Wisconsin wide flanged bulb-tee bridge girder; 72W = 72 in. deep Wisconsin wide flanged bulb-tee bridge girder; DB = debonding ratio; f_{pu} = ultimate capacity of strands. 1 in. = 25.4 mm.

as measured from the centerline and bottom of the girder, respectively (Fig. 2). When calculating the splitting resistance, the prestressing force P_r in $h/4$ (where h is the girder depth) was calculated neglecting the debonded strands.

Instrumentation

Strains in reinforcing bars and concrete were measured where end cracks were expected from analyses. Strain gauges were also placed on strands at 8, 20, and 36 in. (203.2, 508, and 914.4 mm) from the girder end along the strand length to measure the effective transfer length. **Figure 3** shows the locations of gauges on the strands, on end reinforcing bars, and in the concrete. Electric resistance surface gauges (S) were used on the strands and the reinforcing bars. Vibrating-wire strain gauges (VW) were embedded in the concrete to obtain concrete strains directly. Strains were continuously measured during detensioning of all girders.

Results on strand-concrete bond

Figure 4 shows the change in strand strain at the ends of 72W and 54W girders due to detensioning to demonstrate the effective prestress transfer length. Negative strain change occurred with a drop in strand tension. The strain change at the girder end was calculated assuming the end of the strand was free to slip. The strands were tensioned to 75% of the strand ultimate strength.

Strands on the girders with and without debonding had nearly identical values of strain change for both girders. The strand strain gauges at 8 in. (203.2 mm) from the ends of 54W-0%DB and 54W-62%DB malfunctioned and were not shown in Fig. 4. The change in strain along the strand was nonlinear in both girders, indicating a nonuniform bond stress distribution. The measured bond stress was used in the validation of girder analyses.

Strains in reinforcing bars and concrete

Results for 72W girders

Gauges on reinforcing bars were placed in the expected horizontal web-cracking region (S1 to S6), in the inclined cracking region (S7 to S9), and in the Y-cracking region (S10 to S13). **Figure 4** shows the locations of these gauges.

Figure 5 shows the change in strains in reinforcing bars due to detensioning. The measurements from S9 in 72W-0%DB were excluded from Fig. 5 because this gauge malfunctioned during the test. A strain of $690 \mu\epsilon$ corresponds to the 20 ksi (138 MPa) limit on splitting zone reinforcement from section 5.10.10.1 of the AASHTO LRFD specifications for crack control and was provided in Fig. 5 for comparison with the measured strains.

Figure 5 shows that reinforcing bars have a similar strain trend with or without debonding during detensioning. All strains, except at locations S3 (web-crack region) and S13 (Y-crack region), decreased or stayed the same at 25% debonding compared with a bonded girder. The largest decrease and increase in reinforcing bar strain due to debonding was 89% at S10 and 136% at S13, respectively, in the Y-crack region. The average decrease in strains was 13%, 77%, and 4% for web, inclined, and Y-crack regions, respectively. The gauges placed to capture the bar strains near the inclined crack region seem to have missed the actual crack locations, and the measured values were small (less than $60 \mu\epsilon$).

Although the splitting reinforcement was designed to meet the AASHTO LRFD specifications, strains in reinforcing bars closest to the bonded girder end exceeded the AASHTO LRFD specifications limit. Bar strains remained below the limit for the girder, with 25% debonded strands. Strain results

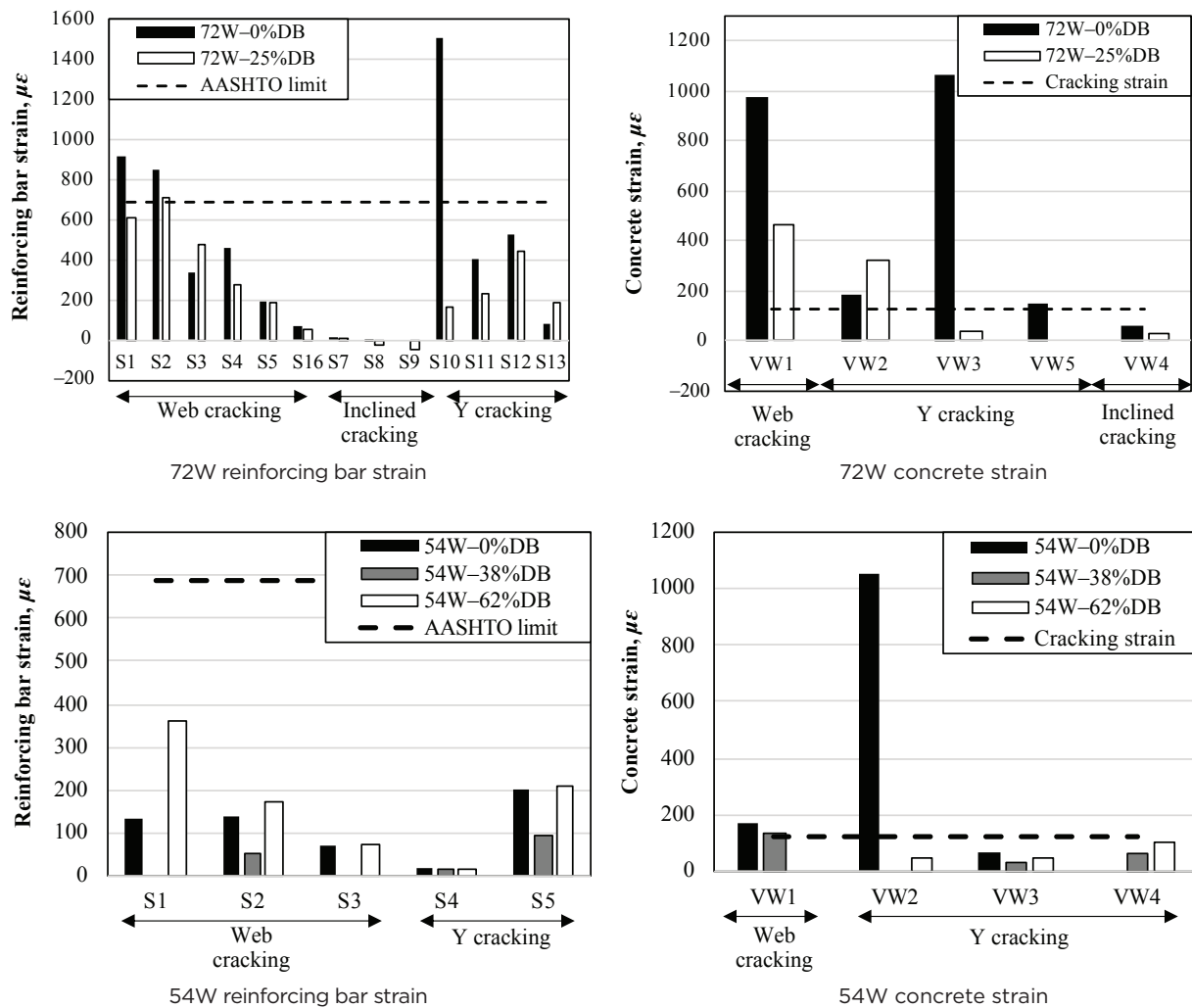


Figure 5. Reinforcing bar and concrete strain measurements in 72W and 54W girders. Note: 54W = 54 in. deep Wisconsin wide flanged bulb-tee bridge girder; 72W = 72 in. deep Wisconsin wide flanged bulb-tee bridge girder; AASHTO = American Association of State Highway and Transportation Officials; DB = debonding ratio; S = electric resistance surface gauge; VW = vibrating-wire strain gauge. 1 in. = 25.4 mm.

also showed that splitting reinforcement stresses were highest in the bars closest to the girder end (S1–3 and S10) and rapidly decreased for bars away from the girder end.

The highest strain was observed in the Y-crack region at the strain gauge S10 on the single transverse bar. This bar was placed for bottom-flange confinement at the very end of 72W-0%DB. This single transverse no. 3 (10M) bar (Fig. 3) appeared to have actively restrained the Y crack in the bonded girder. For 72W-25%DB, the Y-crack strain in the same bar decreased considerably, by 70%. Debonding may have had a significant impact on controlling the Y crack. Strains in bottom-flange lower confinement reinforcement (S13) were small in both girders.

Vibrating-wire gauges were embedded in the concrete near the inclined crack region (VW4), horizontal web-crack

region (VW1), and expected Y-crack region (VW2, VW3, and VW5). Fig. 5 shows the strain changes measured. These strains can be compared with the 126 $\mu\epsilon$ tensile strain limit at which concrete is expected to crack, shown with a dotted line in Fig. 5. Gauge VW5 of the girder with debonding malfunctioned, and its measurements were omitted from the results.

The measured vertical tensile strain in the concrete for the lower web region (VW1) of the girder with debonding was 54% less than that of the girder without debonding (Fig. 5). In both beams, however, the web-cracking strain was still above the 126 $\mu\epsilon$ level at which a horizontal web crack is expected. On average, concrete strains were reduced by 52%, 55%, and 12% in web, inclined, and Y-cracking regions, respectively, due to 25% debonding.

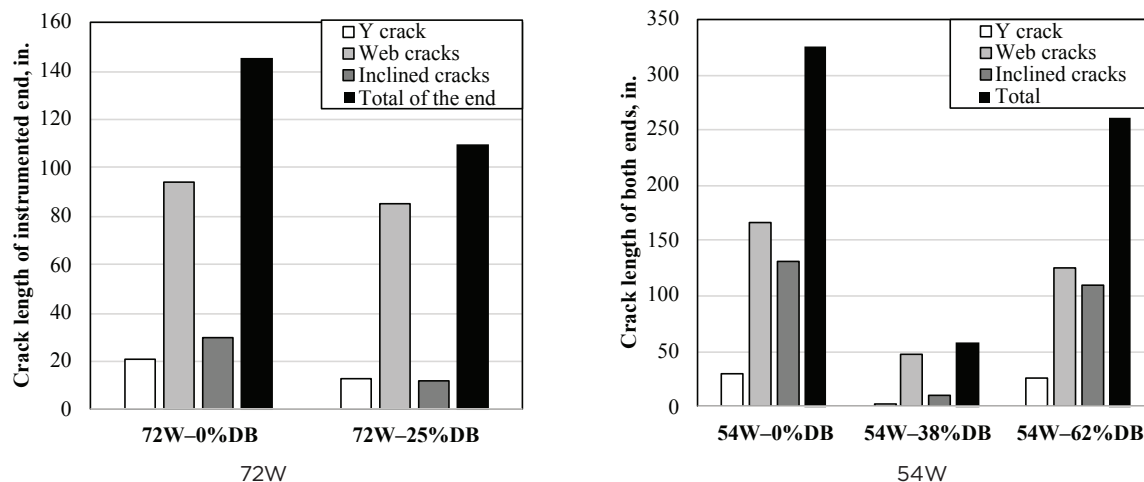


Figure 6. Total crack lengths in 72W and 54W girders. Note: 54W = 54 in. deep Wisconsin wide flanged bulb-tee bridge girder; 72W = 72 in. deep Wisconsin wide flanged bulb-tee bridge girder; DB = debonding ratio. 1 in. = 25.4 mm.

The strains measured by VW2 and VW3, indicators of bottom-flange Y cracking, showed that there was little difference between the two beams at the VW2 (first stirrup) location. At the VW3 (third stirrup) location, however, the bonded beam had strains nearly 21 times greater than the debonded beam. This difference suggests that Y cracks may be induced by strains developing inside the end of the beam as more pre-stress is transferred to concrete.

Results for 54W girders

On average, reinforcing bar and concrete strains in the 54W girders were smaller than the ones measured on the 72W girders. Fig. 5 compares the measured strains in 54W girders with and without debonding on reinforcing bars and in concrete. Figure 3 shows locations of strain gauges on reinforcing bars in web-cracking (S1 through S3) and Y-cracking (S4 through S5) regions and in concrete in web-cracking (VW1) and Y-cracking (VW2 through VW4) regions. Gauges S1 and S3 in 54W-38%DB and VW1 in 54W-62%DB, VW2 in 54W-38%DB, and VW4 in 54W-0%DB malfunctioned, and therefore their results were omitted.

Figure 5 shows that all reinforcing bar strains are below the AASHTO LRFD specifications limit. This indicates that strain gauges were not near crack locations or that reinforcement was not effective in these locations. Observation of Y cracking near S4 indicated that the short and epoxy-coated bar S4 was placed on may not have been efficient. In general, 38% debonding decreased and 62% debonding increased reinforcing bar strains that were already small.

Figure 5 shows concrete strains measured during detensioning with the predicted cracking strain of concrete. From

the measured strains, horizontal cracks can be expected for 54W-0%DB and 54W-38%DB in the web.

In the Y-cracking region, strains in 54W-0%DB jumped to magnitudes well above cracking after the middle strands in the bottom row were detensioned. On the other hand, 54W-62%DB had strains that were 96% of those for 54W-0%DB at the VW2 gauge location. These strains were below the cracking limit. Gauges VW3 and VW4 were placed 14 and 26 in. (355.6 and 660.4 mm) into the girders and measured small (less than $110 \mu\epsilon$) strains. This may indicate that Y cracks do not propagate this far into the girder end.

Crack measurements

After the girders were moved out of the prestressing bed, the number, width, and length of cracks were documented. It was observed that crack lengths and widths increased as the girders were lifted. Crack lengths were measured at one end of the 72W girders and at both ends of the 54W girders.

Cracks in 72W girders

In the 72W girder, 25% debonding did not change the number of cracks compared with 0% debonding. However, 25% debonding decreased both the crack lengths and the maximum crack widths, particularly for Y cracks. The maximum crack width in the bonded girder was relatively large (0.0197 in. [0.5 mm]) and was for a Y crack. Debonding 25% of the strands reduced the maximum crack width of the Y cracks by more than half. **Figure 6** shows crack lengths for the 72W girder. The total length of cracks was reduced 25% by debonding 25% of the strands. Crack lengths particularly decreased in the inclined and Y-crack regions of the debonded girders.

Cracks in 54W girders

Figure 6 shows that debonding 38% and 62% of the strands for girder 54W led to a reduction in total crack length of 83% and 20%, respectively. The strands were debonded for only 8 in. (203.2 mm) from the end for 62% debonding. Debonding a larger portion of the strands but for only a short distance at the girder end (54W-62%DB) was not nearly as effective in reducing the length of cracks as debonding a smaller portion of strands for longer lengths (54W-38%DB).

A Y crack did not occur in the instrumented ends of 54W-0%DB and 54W-38%DB but did form in the instrumented end of 54W-62%DB. The opposite ends of these girders showed a reverse situation, where a Y crack was observed in 54W-0%DB, but not in 54W-38%DB and 54W-62%DB. This difference may be related to how the girders were detensioned. Girder 54W-62%DB had a longer free length of strands, and the release of energy may have created an additional dynamic force and caused the Y crack in the instrumented end of 54W-62%DB.

Finite element modeling

Finite element modeling was used to expand the variations of strand debonding cases studied experimentally, for example, the debonding percentage and locations (Table 2). The analytical models comprised concrete elements with nonlinear material properties in the end zone, concrete ele-

ments with linear elastic material properties away from the end zone, and reinforcing steel elements with linear elastic material properties throughout the girder. For the linear behavior of concrete and steel reinforcing bar, material properties suggested by the AASHTO LRFD specifications²⁰ were used. Mild reinforcing material was Grade 60. The postcracking range of concrete properties, including strain softening under tension, was given by the *fib Model Code for Concrete Structures 2010*.²⁴

Prestress was simulated by applying uniform transfer stresses on concrete elements adjacent to the strand. This load was applied stepwise, with added transfer stress applied as each strand was cut, to follow the possible development of cracks as detensioning proceeds. Only a quarter of a full girder was modeled taking advantage of symmetry across the girder cross section and length.

Four-node tetrahedral finite elements were used for the nonlinear concrete region and six-node triangular prism elements were used in the linear concrete region. The steel reinforcing bar elements were two-node linear truss elements. A finer mesh size of maximum 1.2 in. (30.5 mm) was used for the nonlinear girder end zone. In the linear zone, the mesh size was varied between 1.2 and 2.0 in. (50.8 mm) with the largest elements near the midspan.

Two types of interactions were used in the models: between concrete and reinforcing steel and between the bottom surface

Table 2. Principal tensile strains in the Y-crack region due to effective debonding ratios for finite element analysis of 72W and 54W girders

Total number of strands	Number of draped strands	Debonding ratio, %	Number of bonded strands at bottom flange	Horizontal eccentricity e_h , in.	Vertical eccentricity e_v , in.	Maximum principal tensile strains at bottom-middle of bulb, $\mu\epsilon$		
						72W	54W	Average
48	8	50	16	7.75	2.83	134	n/a	n/a
46	8	48	16	7.75	2.50	120	n/a	n/a
44	8	45	16	7.75	2.50	125	n/a	n/a
42	8	43	16	7.00	2.50	77	96	87
40	8	40	16	7.50	2.50	97	104	101
38	8	42	14	7.86	2.18	115	110	113
36	8	39	14	8.14	2.18	77	121	99
34	8	29	16	8.00	2.33	110	135	123
32	8	31	14	7.57	2.00	84	102	93
30	6	33	14	7.57	2.20	88	98	93
28	6	29	14	8.14	2.00	106	130	118
26	6	23	14	8.43	2.00	124	140	132

Note: 54W = 54 in. deep Wisconsin wide flanged bulb-tee bridge girder; 72W = 72 in. deep Wisconsin wide flanged bulb-tee bridge girder; n/a = not applicable. 1 in. = 25.4 mm.

of the girders and formwork. Reinforcing steel elements were embedded in concrete. For the interaction between the girder bottom and formwork, a surface-to-surface contact definition was used with small sliding formulation. The formwork was modeled as a horizontal surface at the bottom of girders. The contact definition allows the girder to lift up (hard contact with separation in the normal to surface direction) and slide (frictionless in tangential direction) with respect to formwork. Modeling formwork was necessary to prevent the girder from deflecting downward under gravity loading. Representations of finite element analysis modeling of girder and nonlinear material behavior of concrete elements are shown in **Fig. 7**. Additional details and validation of the modeling techniques are provided in previous research.^{18,25}

Finite element analysis validation

Finite element analysis modeling techniques were validated using data collected on 72W and 54W girders. **Figure 8** compares reinforcing bar strains measured in the field tests and predicted

through finite element analyses for both 72W and 54W girders. In general, the finite element analyses and test results were in good agreement for both 72W-0%DB and 72W-25%DB. The largest error for 72W-0%DB was 233% at gauge S13; the largest error for 72W-25%DB was 37% at gauge S1. The mismatch in strains was likely due to a horizontal web crack occurring near the location of the strain gauge that created a high local strain in the bar. An acceptable correlation was achieved between the predicted and measured strains in 54W girders (**Fig. 8**). Similarly to the 72W girders, finite element analysis and test results deviated at two locations, with a maximum error of 122% at S1 for 54W-0%DB.

Figure 8 compares concrete strains from finite element analyses and vibrating-wire gauge measurements for 72W and 54W girders with varying debonding ratios. Overall, the finite element analysis and test results were within 20% of each other except at two locations—VW2 and VW5—in both girders. This was deemed acceptable, considering the heterogeneity of concrete, which could not be modeled at this scale.

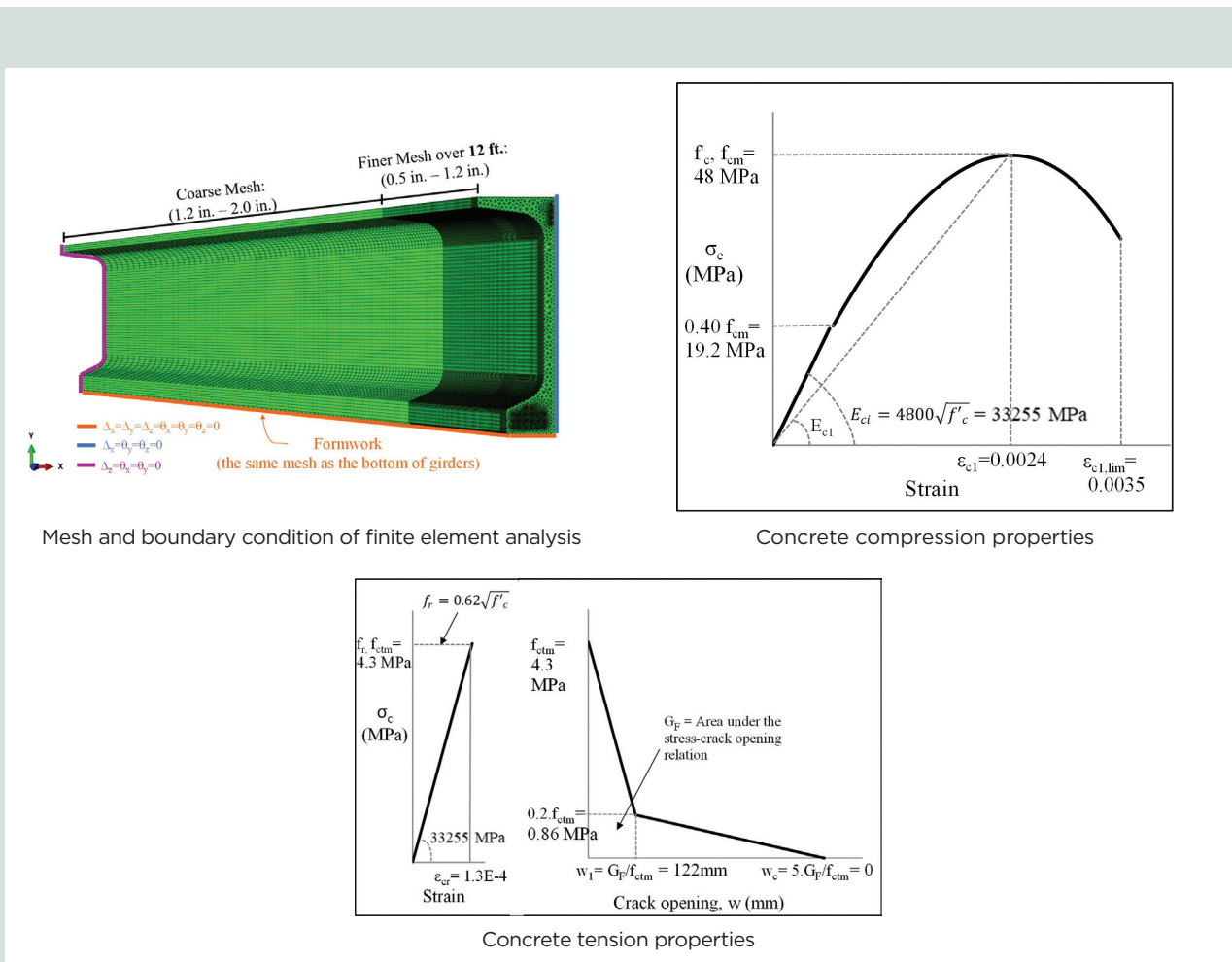


Figure 7. Mesh and boundary condition of finite element analysis, concrete compression properties, and concrete tension properties. Note: E_{c1} = secant modulus from origina to the peak; E_{ct} = tangent modulus; f'_c = concrete compressive strength; f_{cm} = mean value of compressive strength; f_{ctm} = mean tensile strength of concrete; f_r = tensile strength; w_1 = crack opening for $\sigma_{ct} = 0.20f_{ctm}$; w_c = crack opening for $\sigma_{ct} = 0$; ϵ_{c1} = strain at maximum compressive stress; $\epsilon_{c1,lim}$ = ultimate strain; ϵ_{cr} = strain at maximum tensile stress; σ_c = concrete stress; σ_{ct} = concrete tensile stress. 1 in. = 25.4 mm; 1 mm = 0.0394 in.; 1 ft = 0.305 m; 1 MPa = 0.145 ksi.

Effective debonding ratios

Finite element analysis models were used to simulate girder behavior to find an efficient number and location of strands to debond to avoid Y cracking (Table 2). The models were created for the typical strand configurations of 72W and 54W girders used by WisDOT with the maximum lengths of girders allowed for each strand pattern. All debonding patterns included staggered debonding lengths for 3, 6, and 9 ft (914.4, 1828.8, and 2743.2 mm) similar to girder 54W-38%DB (Fig. 2). The concept of debonding an entire set of strands for a short distance of 8 in. (203.2 mm) was used in the experimental study (54W-62%DB) to create a relatively unstressed end block that restrains the girder, similar to the end blocks that were traditionally used with older I-girders that had

thickened webs at the girder ends. However, WisDOT was not interested in pursuing this type of design until additional experimental investigation of crack reduction and impact on end shear strength was completed. Therefore, this strand configuration was not investigated by finite element analysis.

The innermost strands of each row were left bonded to decrease force eccentricity across bottom-flange width. Debonding of the outermost strand column is not currently allowed by the AASHTO LRFD specifications, and therefore these strands were left bonded while selecting the debonding patterns. Concrete strength at detensioning was 7000 psi (48 MPa). All strands were 0.6 in. (15.2 mm) diameter with an initial prestress force of 40 kip (178 kN) considering initial losses. Mild reinforcing material was Grade 60.

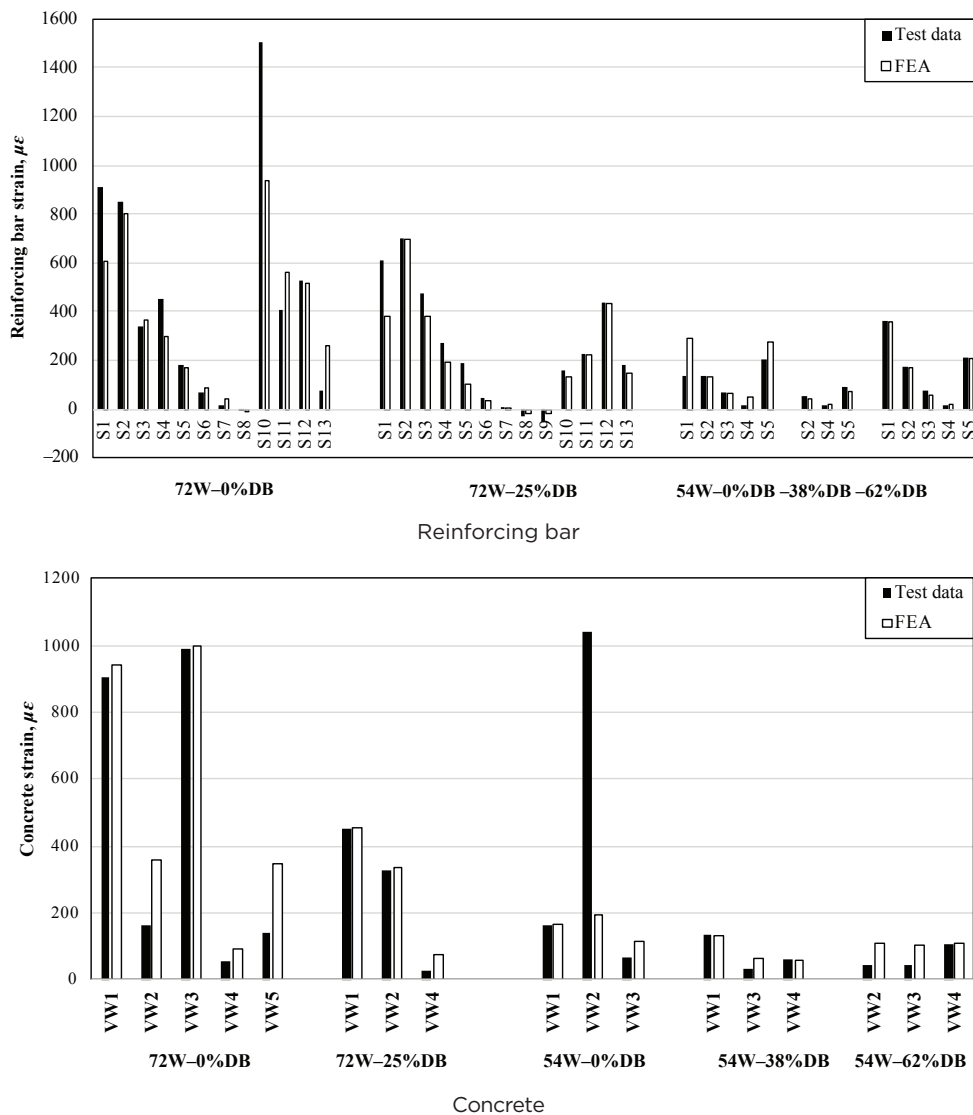


Figure 8. Reinforcing bar and concrete strain comparisons between test data and FEA for 72W and 54W girders. Note: 54W = 54 in. deep Wisconsin wide flanged bulb-tee bridge girder; 72W = 72 in. deep Wisconsin wide flanged bulb-tee bridge girder; DB = debonding ratio; FEA = finite element analysis; S = electric resistance surface gauge. 1 in. = 25.4 mm.

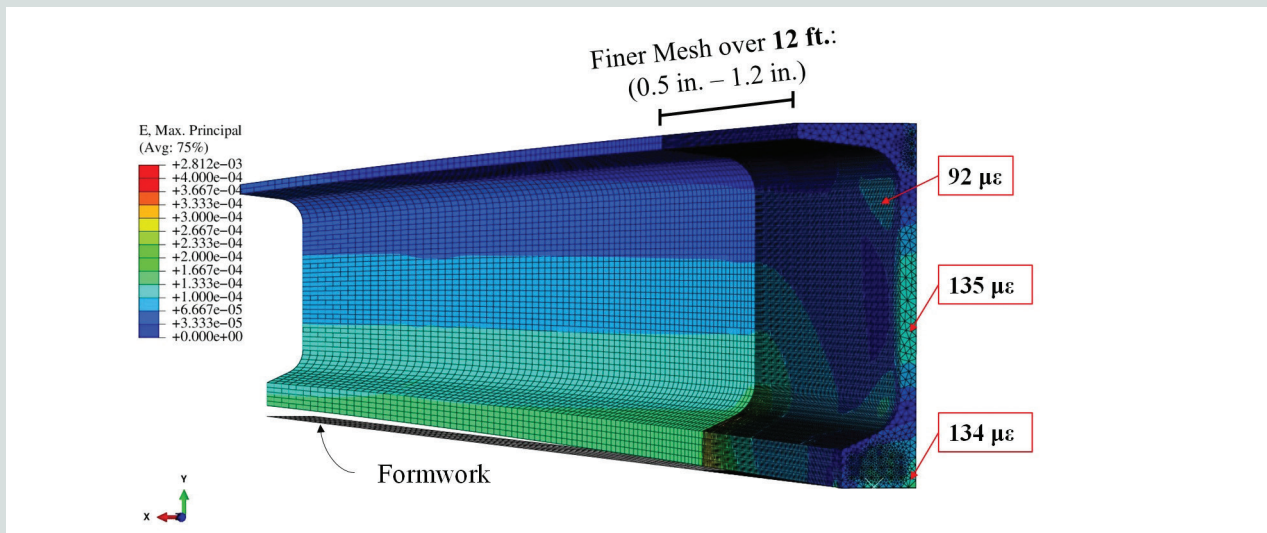


Figure 9. Principal tensile strains of 72W-50%DB. Note: 1 in. = 25.4 mm; 1 ft = 0.305 m.

Table 2 gives ratios of debonding that kept concrete tensile strains in the bottom flange near or below $130 \mu\epsilon$. This strain is associated with concrete rupture stress given by the AASHTO LRFD specifications²⁰ C5.4.2.7. Table 2 also gives the resultant transfer force location of the bonded strands, in other words, the horizontal eccentricity (e_h in Fig. 2) and vertical eccentricity (e_v in Fig. 2) of the resultant strand forces in the bottom flange of the girder. A representative contour plot of principal tensile strains for 72W-50%DB is shown in Fig. 9.

The analysis results showed that the desired debonding ratio and the maximum principal tensile strains within the Y-crack region were similar for 72W and 54W when the number of bonded strands was the same. Table 2 gives the maximum principal tensile strains at 72W and 54W girders in the middle bottom of the bulb (near the Y-crack region). It also shows the average of the maximum principal tensile strains of 72W and 54W near the Y-cracking region. Analysis of girders with different depths but the same bottom flange dimensions and the debonding patterns verified that Y cracks depend on the horizontal eccentricity of resultant forces from the prestress transfer on each side of the bottom flange and are not significantly influenced by the depth of the girder. The number of bonded strands in the bottom flange ranged from 14 to 16 strands. Other details of the girders are provided by Kizilarlan.¹⁸

Prediction of bottom-flange strains

Figure 10 shows correlations between Y-crack tensile strains, prestress force from bonded strands at the ends of girders P_{bonded} , horizontal eccentricity e_h (Fig. 2), and vertical eccentricity e_v (Fig. 2) for the debonding cases studied for 54W and 72W girders. It shows maximum principal tensile strains near the Y-crack region as a function of the following: P_{bonded} , e_h , $P_{bonded}e_h$, and $P_{bonded}e_h e_v$. A regression line is also shown in

this figure, with corresponding R^2 values. Values of R^2 close to 1.00 indicate a strong linear correlation. None of these cases had a strong linear correlation with the principal tensile strain magnitude in the Y-crack region. Among all cases, the best linear correlation was with $P_{bonded}e_h$ with an R^2 value of 0.21.

Figure 11 shows Y-crack principal tensile strains as a function of $P_{bonded}e_h^2$, together with the number of bonded strands used for each analysis. The linear correlation between the principal tensile strain and $P_{bonded}e_h^2$ was the strongest of all other cases studied in Fig. 11. The R^2 value was 0.52. The linear correlation between principal tensile strain and $P_{bonded}e_v^2$ was weak ($R^2 = 0.09$). For a given girder debonding design where P_{bonded} and e_h are known, principal tensile strains in the Y-cracking region can be approximated using the equation in Fig. 11 that assumes a linear correlation with Y-cracking strains: $\epsilon_{Ycrack} = 0.0048P_{bonded}e_h^2 - 65.574$, where ϵ_{Ycrack} is maximum tensile principal strain near the Y crack.

Conclusion

Field tests and finite element analyses were conducted to determine whether debonding strands can successfully control cracks, particularly bottom-flange Y cracks, at the ends of pretensioned girders right after detensioning. The tests were conducted on 72W girders with 0% and 25% debonding ratios and 54W girders with 0%, 38%, and 62% debonding ratios. Test results were used to validate nonlinear finite element analysis models. A parametric study was run using finite element analysis, where girder depth, total number of strands, and debonding ratio were variables. Maximum principal tensile strains around the center of the bottom flange (Y-crack region) were reported. Following are the conclusions of this study:

- Measured strands in girders with and without debonding had similar transfer lengths.

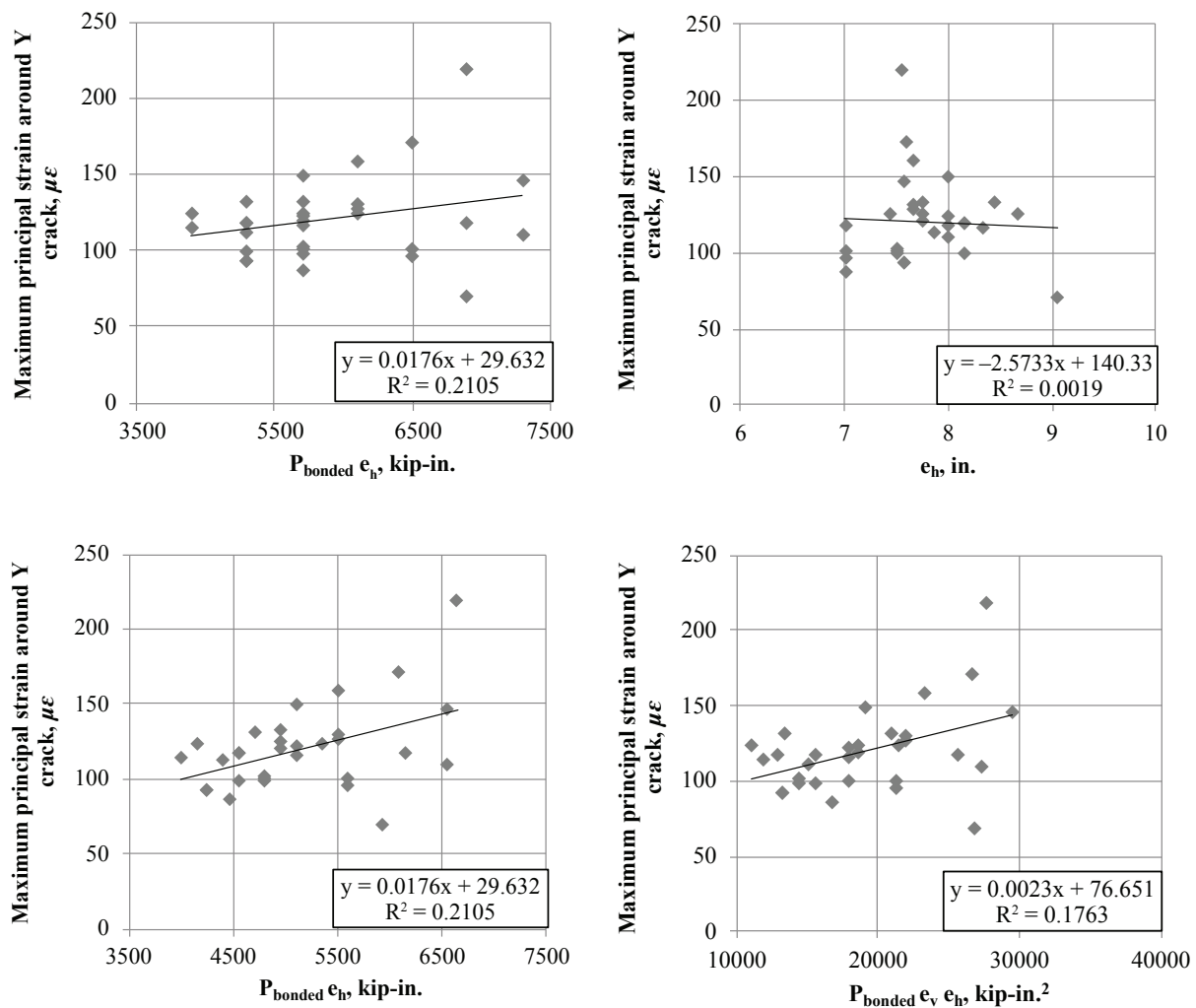


Figure 10. Correlation between Y-crack tensile strains, bonded prestress force, and horizontal and vertical eccentricities. Note: e_h = horizontal eccentricity of the bonded straight strands; e_v = vertical eccentricity of the bonded straight strands from bottom of the girders; P_{bonded} = total prestressing force from bonded strands at the ends of girders; R^2 = linear regression. 1 in. = 25.4 mm; 1 kip = 4.448 kN; 1 kip-in. = 0.113 kN-m.

- Girder instrumentation showed that debonding 25% of strands on the 72W girders reduced average reinforcing bar strains by 13% for the inclined-crack region, 77% for the web-crack region, and 4% for the Y-crack region. Debonding 25% of strands on the 72W girders reduced average concrete strains by 52% for the inclined crack region, 55% for the web-crack region, and 12% for the Y-crack region.
- Field instrumentation showed that debonding 38% of strands on the 54W girders reduced average reinforcing bar strains by 64% for the web-crack region and 30% for the Y-crack region. Debonding 38% of strands on the 54W girders reduced average concrete strain by 19% for the web-crack region and 54% for the Y-crack region.
- Field instrumentation showed that debonding 62% of strands for a very short distance ($h/9$) from the ends of the 54W girders increased average reinforcing bar strains by 68% for the web-crack region and 12% for the Y-crack region. Debonding 62% of strands for 54W girders reduced average concrete strains by 64% for the Y-crack region.
- Crack lengths measured during field monitoring were affected by the reduction of concrete strains. For cracks measured at one end of each of the 72W girders, the total crack lengths decreased by 24% with 25% debonding. For cracks measured at both ends of the three 54W girders, the total crack lengths decreased by 82% and 20% with 38% and 62% debonding, respectively.
- Strains obtained by finite element analysis compared reasonably well with measured strains. The average error in reinforcing steel strain prediction was between 8% and

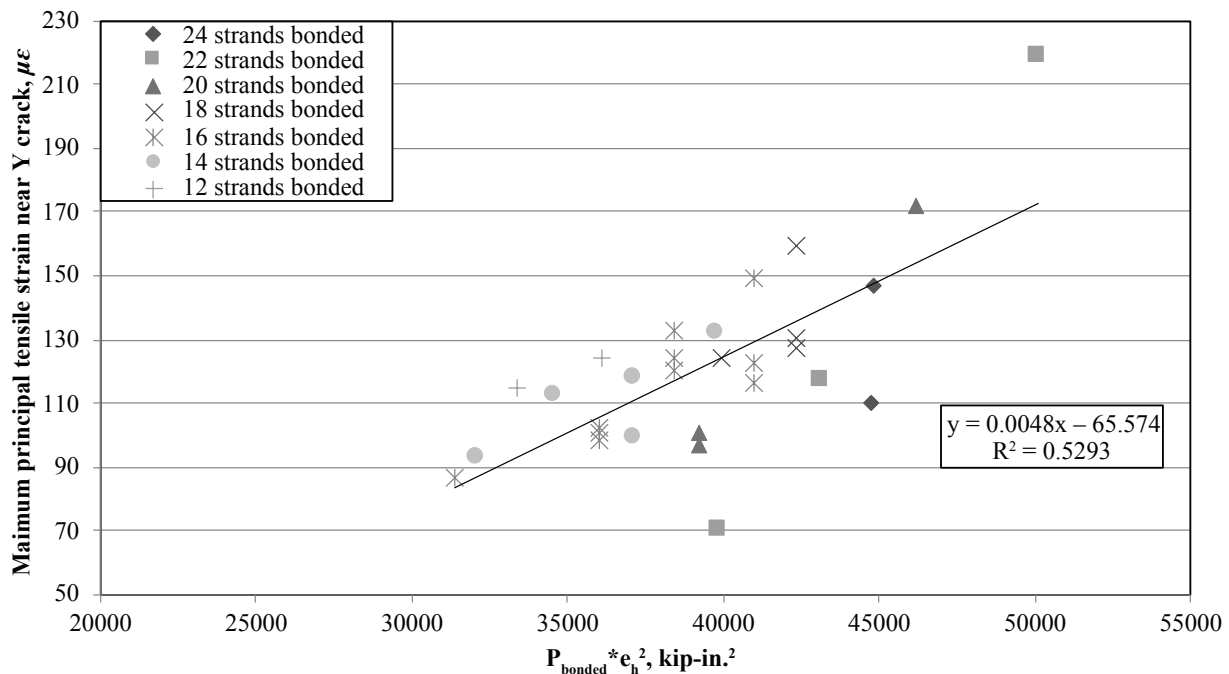


Figure 11. Correlation between Y-crack tensile strains, bonded prestress force, and horizontal eccentricity. Note: e_h = horizontal eccentricity of the bonded straight strands; P_{bonded} = total prestressing force from bonded strands at the ends of girders; R^2 = linear regression. 1 kip-in. = 0.113 kN-m.

66%. The average error in concrete strain prediction was 36% and 92%. High errors were attributed to localized peaks measured by small and finite-length strain gauges.

- Analyses showed that Y cracks at the ends of the WisDOT bulb-tee girders were induced by resultant prestress forces developed in the two overhanging portions of the girder bottom flanges and their eccentricity from the center of the flange. The direction of the tensile strains in the bottom flange caused by prestress transfer matched the shape and locations of observed Y cracks.
- The results of the parametric analyses on two girders (72W and 54W) showed that debonding patterns, with careful consideration of strand selection for debonding, could reduce concrete tension strains to a level below the expected elastic cracking limit in the crack-prone zones. For most cases, debonding ratios were greater than 25%. The debonding lengths were the same as those used in the 54W-38% girder. In the 54W-38% girder, each strand group was debonded for at least 3 ft (914.4 mm) and there was at least 3 ft between locations of termination of debonding.
- Correlations were investigated between maximum principal tensile strains in the bottom flange (potentially causing Y cracks) and prestress force from bonded strands, eccentricity of bonded prestress force in the vertical direction, eccentricity of bonded prestress force in the horizontal

direction on one side of the bottom flange, and combinations of these. The strongest correlation between principal tensile strains was with the bonded prestress force multiplied by the square of the horizontal eccentricity of the bonded prestress force on one side of the bottom flange ($R^2 = 0.53$). This correlation can be assumed to be linear. A simple equation to predict Y crack strains based on bonded prestress force and horizontal eccentricity of strands is proposed: $\epsilon_{Ycrack} = 0.0048P_{bonded}e_h^2 - 65.574$. Therefore, the maximum principal strain can be estimated by inputting the bonded prestressing force P_{bonded} and the horizontal eccentricity of the bonded strands about the centerline of the cross section of girders e_h .

Acknowledgments

This research was funded through the Wisconsin Highway Research Program by WisDOT and the Federal Highway Administration under project 0092-16-05. The contents of this paper reflect the views of the authors, who are responsible for the facts and accuracy of the data presented herein. The contents do not necessarily reflect the official views of WisDOT or the Federal Highway Administration. Assistance provided by WisDOT personnel, particularly research chairs William Oliva and David Kiekbusch, is greatly appreciated. Spancrete and County Materials precast concrete operations provided the researchers access and assistance at their facilities during fabrication and detensioning of test girders.

References

1. Crispino, E. D., T. E. Cousins, and C. L. Roberts-Wollmann. 2009. "Anchorage Zone Design for Pretensioned Precast Bulb-T Bridge Girders in Virginia." FHWA/VTRC 09-CR15. Charlottesville, VA: Virginia Transportation Research Council. http://www.virginia.gov/vtrc/main/online_reports/pdf/09-cr15.pdf.
2. Tadros, M. K., S. S. Badie, and C. Y. Tuan. 2010. *Evaluation and Repair Procedures for Precast/Prestressed Concrete Girders with Longitudinal Cracking in the Web*. Washington, DC: Transportation Research Board.
3. Gamble, W. L. 1970. *Field Investigation of a Continuous Composite Prestressed I-Beam Highway Bridge Located in Jefferson County, Illinois*. Springfield, VA: National Technical Information Service.
4. Marshall, W. T., and A. H. Mattock. 1962. "Control of Horizontal Cracking in the Ends of Pretensioned Prestressed Concrete Girders." *PCI Journal* 7 (5): 56–74.
5. Gergely, P., and M. A. Sozen. 1967. "Design of Anchorage-Zone Reinforcement in Prestressed Concrete Beams." *PCI Journal* 12 (2): 63–75.
6. Tan, K., K. Tong, and C. Tang. 2001. "Direct Strut-and-Tie Model for Prestressed Deep Beams." *Journal of Structural Engineering* 127 (9): 1076–1084.
7. Harries, K. A., B. M. Shahrooz, B. E. Ross, P. Ball, and H. R. Trey. 2018. "Modeling and Detailing Pretensioned Concrete Bridge Girder End Regions Using the Strut-and-Tie Approach." *Journal of Bridge Engineering* 24 (3). [https://doi.org/10.1061/\(ASCE\)BE.1943-5592.0001354](https://doi.org/10.1061/(ASCE)BE.1943-5592.0001354).
8. Okumus, P., and M. G. Oliva. 2013. "Evaluation of Crack Control Methods for End Zone Cracking in Prestressed Concrete Bridge Girders." *PCI Journal* 58 (2): 91–105.
9. Okumus, P., and M. G. Oliva. 2014. "Strand Debonding for Pretensioned Bridge Girders to Control End Cracks." *ACI Structural Journal* 111 (1): 201–210.
10. Okumus, P., M. G. Oliva, and S. Becker. 2012. "Non-linear Finite Element Modeling of Cracking at Ends of Pretensioned Bridge Girders." *Engineering Structures* 40: 267–275.
11. Okumus, P., R. P. Kristam, and M. Diaz Arancibia. 2016. "Sources of Crack Growth in Pretensioned Concrete-Bridge Girder Anchorage Zones After Detensioning." *Journal of Bridge Engineering* 21 (10). [https://doi.org/10.1061/\(ASCE\)BE.1943-5592.0000928](https://doi.org/10.1061/(ASCE)BE.1943-5592.0000928).
12. Arab, A., S. S. Badie, M. T. Manzari, B. Khaleghi, S. J. Seguirant, and D. Chapman. 2014. "Analytical Investigation and Monitoring of End-Zone Reinforcement of the Alaskan Way Viaduct Super Girders." *PCI Journal* 59 (2): 109–128.
13. Ronanki, V. S., D. I. Burkharter, S. Aaleti, W. Song, and J. A. Richardson. 2017. "Experimental and Analytical Investigation of End Zone Cracking in BT-78 Girders." *Engineering Structures* 151: 503–517.
14. Van Meirvenne, K., W. De Corte, V. Boel, and L. Taerwe. 2018. "Non-Linear 3D Finite Element Analysis of the Anchorage Zones of Pretensioned Concrete Girders and Experimental Verification." *Engineering Structures* 172: 764–779.
15. Tuan, C. Y., S. A. Yehia, N. Jongpitaksseel, and M. K. Tadros. 2004. "End Zone Reinforcement for Pretensioned Concrete Girders." *PCI Journal* 49 (3): 68–82.
16. Ross, B. E., M. D. Willis, H. Hamilton, and G. R. Consolazio. 2014. "Comparison of Details for Controlling End-Region Cracks in Precast, Pretensioned Concrete I-Girders." *PCI Journal* 59 (2): 96–108.
17. O'Callaghan, M. R., and O. Bayrak. 2007. "Tensile Stresses in the End Regions of Pretensioned I-Beams at Release." MSE thesis. University of Texas at Austin, Austin, TX.
18. Kizilarlan, E. 2016. "De-bonding Strands as an Anchorage Zone Crack Control Method for Pretensioned Concrete Bulb-tee Bridge Girders Using Nonlinear Finite Element Analysis." MS thesis, University of Wisconsin–Madison, Madison, WI.
19. Dunkman, D. A., C. G. Hovell, A. M. Moore, A. Aven-dano, O. Bayrak, and J. O. Jirsa. 2010. "Bursting and Spalling in Pretensioned Concrete Beams." In: *Third International fib Congress and PCI Annual Convention & Bridge Conference: Proceedings, May 29–June 2, 2010, Washington, DC*. Chicago, IL: PCI.
20. AASHTO (American Association of State Highway and Transportation Officials). 2018. *AASHTO LRFD Bridge Design Specifications*. Washington, DC: AASHTO.
21. Kannel, J., C. E. French, and H. K. Stolarski. 1997. "Release Methodology of Strands to Reduce End Cracking in Pretensioned Concrete Girders." *PCI Journal* 42 (1): 42–54.
22. Willis, M. 2014. "Post-Tensioning to Prevent End-Region Cracks in Pretensioned Concrete Girders." MS thesis, Clemson University, Clemson, SC.

23. WisDOT (Wisconsin Department of Transportation). "Bridge Manual Standard Drawings." *Bridge Manual*. Madison, WI: WisDOT. <https://wisconsindot.gov/Pages/doing-bus/eng-consultants/cnslt-rsrcs/strct/bridge-manual-standards.aspx>.
24. *fib* (International Federation for Structural Concrete). 2013. *fib Model Code for Concrete Structures 2010*. Berlin, Germany: Ernst & Sohn.
25. Okumus, P. 2012. "Nonlinear Analysis of Pretensioned Bridge Girder Ends to Understand and Control Cracking at Prestress Release." PhD diss., University of Wisconsin–Madison, Madison, WI.

$\varepsilon_{c1.lim}$	= ultimate strain
ε_{cr}	= strain at maximum tensile stress
ε_{Ycrack}	= maximum tensile principal strain near Y crack
σ_c	= concrete stress
σ_{ct}	= concrete tensile stress

Notation

e_h	= horizontal eccentricity of the bonded straight strands
e_v	= vertical eccentricity of the bonded straight strands from bottom of the girders
E_{c1}	= secant modulus from origin to the peak,
E_{ci}	= tangent modulus
f'_c	= concrete compressive strength
f_{cm}	= mean value of compressive strength
f_{ctm}	= mean tensile strength of concrete
f_{pu}	= ultimate capacity of strands
f_r	= tensile strength
G_F	= area under the stress-loading condition
h	= girder depth
P_{bonded}	= total prestressing force from bonded strands at the ends of girders
P_r	= prestressing force
R^2	= correlation coefficient of linear regression
w_1	= crack opening for $\sigma_{ct} = 0.20f_{ctm}$
w_c	= crack opening for $\sigma_{ct} = 0$
ε_c	= strain
ε_{c1}	= strain at maximum compressive stress

About the authors



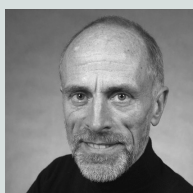
Emre Kizilarслан received his master's degree from the University of Wisconsin–Madison, where he performed experimental and analytical studies on the debonding of prestressed bridge girders. He is a PhD candidate at the State University of New York at

Buffalo. He is conducting experimental research and numerical analysis for to the development of seismic design provisions for coupled steel-plate composite wall systems.



Pinar Okumus is an associate professor in the Department of Civil, Structural and Environmental Engineering at the State University of New York at Buffalo. Her research covers service and extreme event response of reinforced and prestressed

concrete structures to achieve longevity and resiliency. She is a member of PCI.



Michael G. Oliva is a professor emeritus in the Department of Civil and Environmental Engineering at the University of Wisconsin–Madison. He is also a Fellow of PCI.

Abstract

Bulb-tee pretensioned concrete girders are widely used for bridge construction. Cracks, however, are often observed near the anchorage zones of these girders during detensioning and can grow in size during subsequent transportation. The cracks can take various forms, including inclined web cracks, horizontal web cracks, and bottom-flange Y cracks. This study used field measurements and finite element analyses to investigate the impact of debonding on anchorage-zone cracks. Strains in reinforcing bar and concrete were measured and compared in girders with various levels of debonding during detensioning. Debonding 25% of strands in 72 in. (1829 mm) bulb-tee girders and debonding 38% of strands in 54 in. (1372 mm) bulb-tee girders led to reductions in strains of 12% and 54%, respectively. Validated nonlinear analytical models were used to determine efficient numbers and patterns of strands to debond. A linear correlation can be assumed between tensile strains in Y-crack regions and prestress multiplied by the square of the horizontal eccentricity of prestress force on one side of the bottom flange.

Keywords

Bottom-flange Y cracks, bridge girder, girder, girder end cracking, nonlinear finite element analysis, pretensioned girder, strand debonding.

Review policy

This paper was reviewed in accordance with the Precast/Prestressed Concrete Institute's peer-review process.

Reader comments

Please address any reader comments to *PCI Journal* editor-in-chief Tom Klemens at tklemens@pci.org or Precast/Prestressed Concrete Institute, c/o *PCI Journal*, 8770 W. Bryn Mawr Ave., Suite 1150, Chicago, IL 60631. [f](#)